CHEMISTRY

Contorted acene ribbons for stable and ultrasensitive neural probes

Shayan Louie[1]†, Qifeng Jiang[1]*†, Duncan J. Wisniewski[2,3]†, Si Tong Bao[1], Honghu Zhang[4], Kaushik Chivukula[5], Qiyi Fang[5], Ashutosh Garudapalli[5], Scott R. Docherty[1], Fay Ng[1], Michael Steigerwald[1], Yu Zhong[5], Dion Khodagholy[3]*, Colin Nuckolls[1]*

Organic materials that conduct both electrons and ions are integral to implantable bioelectronics because of their conformable nature. There is a dearth of these materials that are highly sensitive to cations, which are the majority ions on the surface of neurons. This manuscript offers a solution using an extended ribbon structure that is defect-free, providing high electronic mobility along its fused backbone, while the edge structure of these ribbons promotes high ionic conductivity. We incorporated these mixed ion/electron conductors into neural probes and implanted them in a rodent brain where they offer a suite of useful properties: high cation sensitivity, stability over several weeks after implantation, and biocompatibility. These materials represent an innovative class of implantable biosensors.

INTRODUCTION

As neuroscience advances, a new generation of organic mixed ionic/electronic conductors (OMIECs) is critical for enhancing the sensitivity and stability of neural activity recording devices (*1*–*3*). The signal transduction of the ionic flux–based communication between neurons is often carried out using microelectrode interfaces (*4*). A critical aspect of studying the complex in vivo interactions between neurons is the ability to monitor both cations and anions. Cations are particularly important for neural sensing due to their prevalence on the surface of neurons relative to anions (*4*). Monitoring their participation in the generation and propagation of action potentials provides valuable information regarding the ongoing neural activity and is essential for the advancement of medical diagnostics and intervention.

Now, hole transporting or p-type OMIECs are the dominant conducting polymers for in vivo electrophysiology due to their stable, biocompatible, and nontoxic nature (*5*–*8*). Among this group, poly(3,4-ethylenedioxythiophene) polystyrene sulfonate (PEDOT:PSS) has received wide attention in the field of bioelectronics owing to its high conductivity, excellent electrochemical stability, low toxicity, and commercial availability (*1*, *3*, *4*, *9*, *10*). Although this material is primarily a hole conductor, it responds to cationic fluxes in electrolytes or biological tissues through hole-density alterations along the PEDOT backbone facilitated by the anionic PSS.

Electron transporting or n-type OMIECs are responsive to cations and can directly transduce ionic fluctuations through their backbones. However, their implementation in neural sensing is hindered by low electron mobilities, slow response speeds, and poor durability—often resulting from thermodynamic instability under ambient conditions (*3*, *4*, *11*). Developing new n-type materials is crucial to achieving a comprehensive understanding of ion activity in biological systems.

This manuscript describes the first example of such a biosensor for cations that functions for weeks while implanted in a rodent brain. We observe robust neural signals during all stages, including both sleep and awake states. These results demonstrate the reliability of OMIEC bioelectronic interfaces as recording and observation platforms. We anticipate the combination of the current state-of-the-art p-type anion sensitive recording devices with these cation sensitive interfaces will provide more complete observations of neural electrophysiology.

RESULTS

The materials responsible for these recordings are an innovative conjugated ladder polymer—Contorted Acene Ribbon System (CARS) (Fig. 1A)—which has a defect-free, fused backbone providing exceptional electron transport (Fig. 1B) and a contorted/functionalized edge, enabling high ion conduction and biocompatibility (Fig. 1C) (*12*–*15*). The fully fused and functionalized CARS is hundreds of nanometers in length and is easily derivatized, providing a vast genus of n-type OMIEC materials for implantable biosensors. The chemistry we developed to create CARS is shown in Fig. 1D. The key intermediate is a fully fused ladder polymer, the helical perylene tetraester ribbon (hPTR), having an ultralong acene core with more than 500 rings and more than 120 nm in length (fig. S1). Functionalization of hPTR leads to CARS, which is decorated by imides with biocompatible oligoethylene glycol groups. Our approach yields an extended acene backbone that is free of defects, allowing efficient electron transport. Furthermore, the contorted backbone introduces intrinsic nanopores that create space for ion transport (fig. S2). This structural design has been demonstrated to effectively enhance ionic diffusivity in various electrochemical applications, including lithium-ion batteries (*13*), pseudocapacitors (*16*), and organic electrochemical transistors (OECTs) (*17*,*18*). Meanwhile, the oligoethylene glycol sidechains provide hydrophilicity and ion affinity, synergistically facilitating ion transport (Fig. 1C) (*13*, *17*). We also find that the imide groups positioned along the acene ribbon edges lower the energy level of the conduction band, enabling efficient

[1]Department of Chemistry, Columbia University, New York, NY 10027, USA. [2]Department of Electrical Engineering, Columbia University, New York, NY 10027, USA. [3]Samueli School of Engineering, University of California, Irvine, Irvine, CA 92697, USA. [4]National Synchrotron Light Source II, Brookhaven National Laboratory, Upton, NY 11973, USA. [5]Department of Materials Science and Engineering, Cornell University, Ithaca, NY 14853, USA.
*Corresponding author. Email: qj2175@columbia.edu (Q.J.); dion.kh@uci.edu (D.K.); cn37@columbia.edu (C.N.)
†These authors contributed equally to this work.

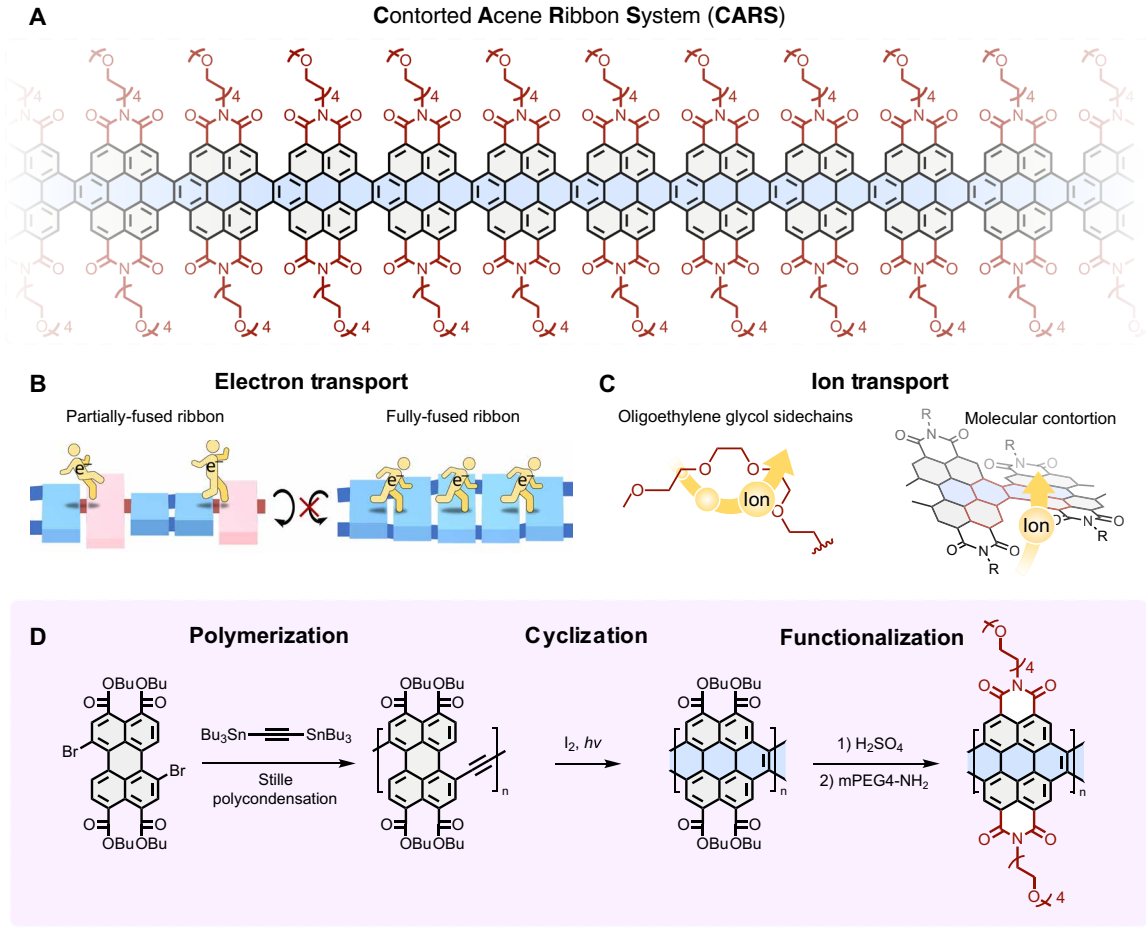

Fig. 1. Contorted Acene Ribbon System. (**A**) Structural core of CARS. (**B**) Electron transport in partially fused versus full-fused ribbons. (**C**) Ion transport pathways in CARS. (**D**) Synthetic strategy for CARS.

electrochemical doping and dedoping that is stable and reversible under ambient, aqueous, and physiological conditions (fig. S3 and table S1).

The mixed conduction properties of CARS make it promising for sensing biological events involving controlled ionic fluxes (*4*). To evaluate the effectiveness of CARS as a biopotential interface material, it was patterned onto a conformable array of gold electrodes (Fig. 2A) and used to record chronically from a freely moving rodent (Fig. 2B) (*19*). Electrode impedance was found to be low and uniform across the array and comparable to the state-of-the-art p-type material PEDOT:PSS, demonstrating the processability of CARS (Fig. 2C and fig. S4). This electrode uniformity allows the probe to reach a large spatial extent while recording high quality signals. The high spatiotemporal resolution achieved here enables us to identify physiological waveforms throughout the brain and track how they propagate. Cortical oscillations consistent with the characteristics of delta spindles were detected, indicating both high sensitivity and fast response from the CARS-based electrodes (Fig. 2D) (*20*, *21*). These oscillations have been shown to provide substantial information about the consolidation and retrieval of memories (*22*). The acquisition of these high-quality signals makes CARS an ideal candidate for use in neuroscience experimentation.

CARS is an excellent neural interface over all activities of the rodent; this makes it suitable for neural recording across many experimental paradigms. For example, Fig. 2E classifies the neural signals from the CARS biosensor array by frequency content identified sleep states, consistent with rapid eye movement (REM), non-REM (NREM), and a waking state. The recordings were taken in 2-hour sessions for over 2 weeks to evaluate the stability of the device in vivo. Consistent spindle activity was acquired in the NREM sleep state (Fig. 2F) demonstrating the stability of physiological signal acquisition is suitable for chronic and behavioral studies in neuroscience. The electrode impedance measurements in vivo on each day of recording (Fig. 2G) show stable performance, indicating that data maintain a similar quality and are comparable between recording sessions. We note that CARS is the first n-type material showing these long-term and stable high-performance recordings in vivo, and in contrast to PEDOT:PSS, can do so without the aid of any additives. The cation sensitivity of CARS allows it to complement existing p-type conductive polymers by creating a complete picture of neural activity composed of ion fluctuations within the brain (*23*, *24*).

The CARS material at the base of these biosensors demonstrates remarkable performance, showcasing high transduction, fast response, and long-term stability. To probe this, we fabricated OECTs

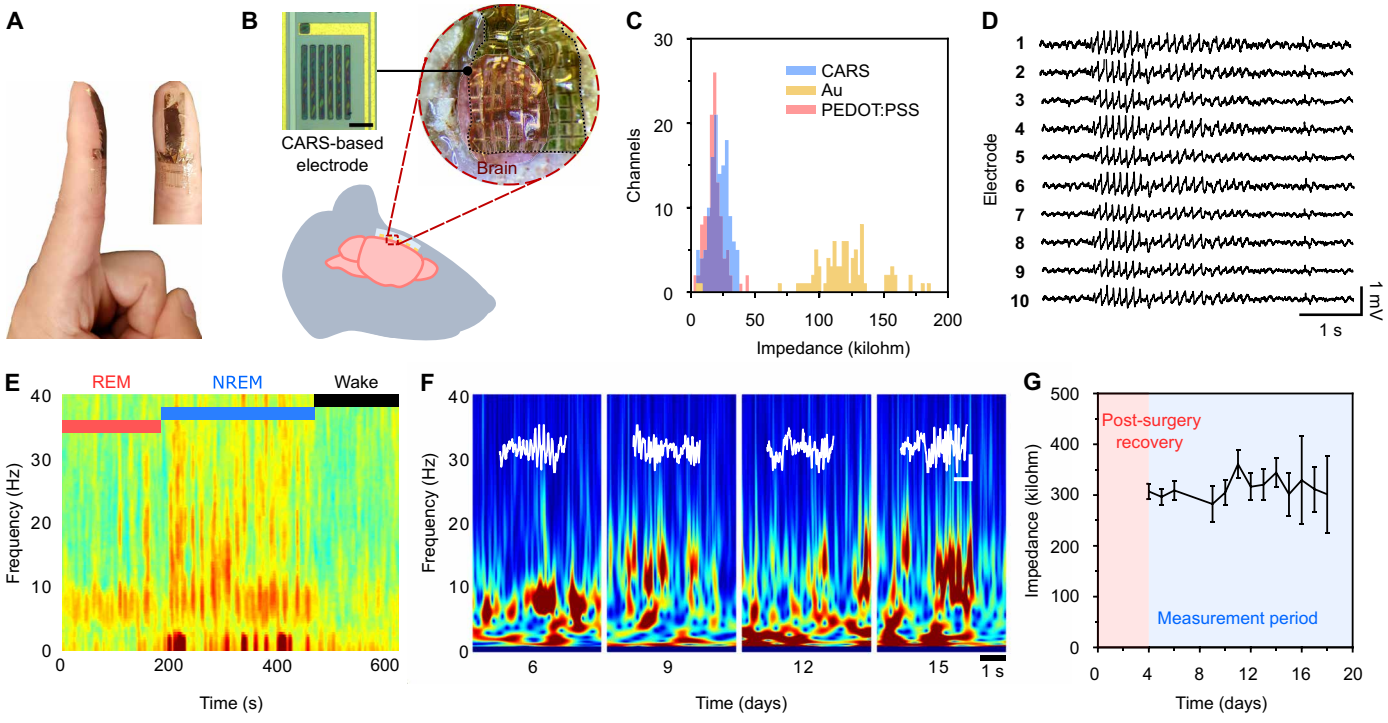

Fig. 2. Stable electrocorticography recording using conformable electrode array. (**A**) Photographs of neural probe arrays conforming to the surface of a finger. (**B**) Micrograph of CARS-based neural probe and placement on the brain of a rat. Colors have been enhanced for clarity. Scale bar, 100 μm. Electrodes are 40 μm by 40 μm with 500-μm interelectrode spacing. (**C**) Channel impedance of uncoated (yellow), commercial PEDOT:PSS-coated (pink) and CARS-coated (blue) electrode arrays at 1 kHz in a three-electrode benchtop setup. (**D**) Delta spindle activity for 10 different devices recorded on day 9 of chronic local field potential (LFP) recording. (**E**) Time-frequency spectrogram of LFP recording on day 9 classified into sleep states. (**F**) Time-frequency spectrogram of LFP recording during nREM sleep across multiple days. Spindle activity from each recording session (white). Scale bar, 500 ms × 250 mV. (**G**) Electrode impedance measurements in vivo from an initial 64 functional channels over 18 days showing mean ± SE.

with CARS as the active material. Their performance is described in Fig. 3. CARS exhibits best-in-class levels of high transconductance ($G_{M,norm.}$ = 40.6 S cm^{-1}) and μC^* (120 F V^{-1} cm^{-1} s^{-1}) (Fig. 3A and table S2) (*25*–*31*), along with a low threshold voltage of 0.26 ± 0.01 V and a high $I_{on/off}$ ratio (>10^6) (Fig. 3, B and C). CARS demonstrates swift τ_{on} and τ_{off} values of 590 ± 70 and 73 ± 39 μs, respectively, upon application of a 0.7-V gate pulse (Fig. 3D) among the best for n-type OECTs (*25*–*32*) and within the timescale sufficient for recording neural activity (*20*, *33*). OECTs incorporating CARS are also highly stable, retaining 87% of their initial current more than 5000 pulsing cycles under ambient/aqueous conditions, which greatly enhances the practical use of this material (Fig. 3E). In addition, these OECTs are highly sensitive to cations, demonstrating current responses to electrolyte ion concentrations well below 100 μM (fig. S5). These results indicate efficient electron transport enabled by a fully fused backbone with excellent π-π overlap and fast ion transport driven by hydrophilic sidechains and molecular contortion (*3*, *13*, *34*, *35*).

The extraordinarily high performance of CARS is due to the perfection in its long and highly conjugated backbone. ^{1}H nuclear magnetic resonance (NMR) spectroscopy of hPTR reveals a defect-free backbone from the singular broad resonance (10.9 parts per million) in the aromatic region from the ortho-protons on perylenes (Fig. 4A). As a point of comparison, we also synthesized a defective ribbon through a typical thermally activated Stille polycondensation that forms homo-coupled diyne subunits as a side product (Fig. 4B) (*36*). We refer to this as defective-CARS (D-CARS). ^{1}H NMR of D-hPTR suggests structural defects (Fig. 4A and fig. S6) on the order of 10%, consistent with previous literature (*36*, *37*). While the ultraviolet-visible (UV-vis) spectrum of CARS has a sharp maximum absorption peak revealing a uniform backbone structure, the UV-vis spectrum of D-CARS shows broader, poorly defined peaks and a 15-nm blueshift relative to CARS (Fig. 4C).

The defects in D-CARS have minimal influence on the ribbons' charge storage properties but a substantial effect on its electron mobility. OECTs incorporating D-CARS exhibit over an order of magnitude lower normalized transconductance of 3.30 ± 0.43 S cm^{-1}. τ_{on} and τ_{off} times are also longer at 1.36 ± 0.32 and 0.31 ± 0.17 ms, respectively (Fig. 4D and fig. S7). We then examined their volumetric capacitances (C^*) and electron mobilities (μ). Both CARS and D-CARS exhibit comparable volumetric capacitances of 203 ± 36 F cm^{-3} (CARS) and 180 ± 16 F cm^{-3} (D-CARS) (Fig. 4E and fig. S8). However, CARS and D-CARS have μ values of 0.59 ± 0.07 and 0.065 ± 0.006 cm^2 V^{-1} s^{-1}, respectively, as calculated from the transfer curves and volumetric capacitances (Fig. 4E and fig. S9) (*38*, *39*). This suggests that variations in backbone integrity create an inherent difference in electron transport between the two acene ribbons.

DISCUSSION

We attribute the high mobility in CARS to efficient intramolecular and intermolecular electron transport through an extended acene backbone with strong π-conjugation (figs. S10 and S11). On the other hand,

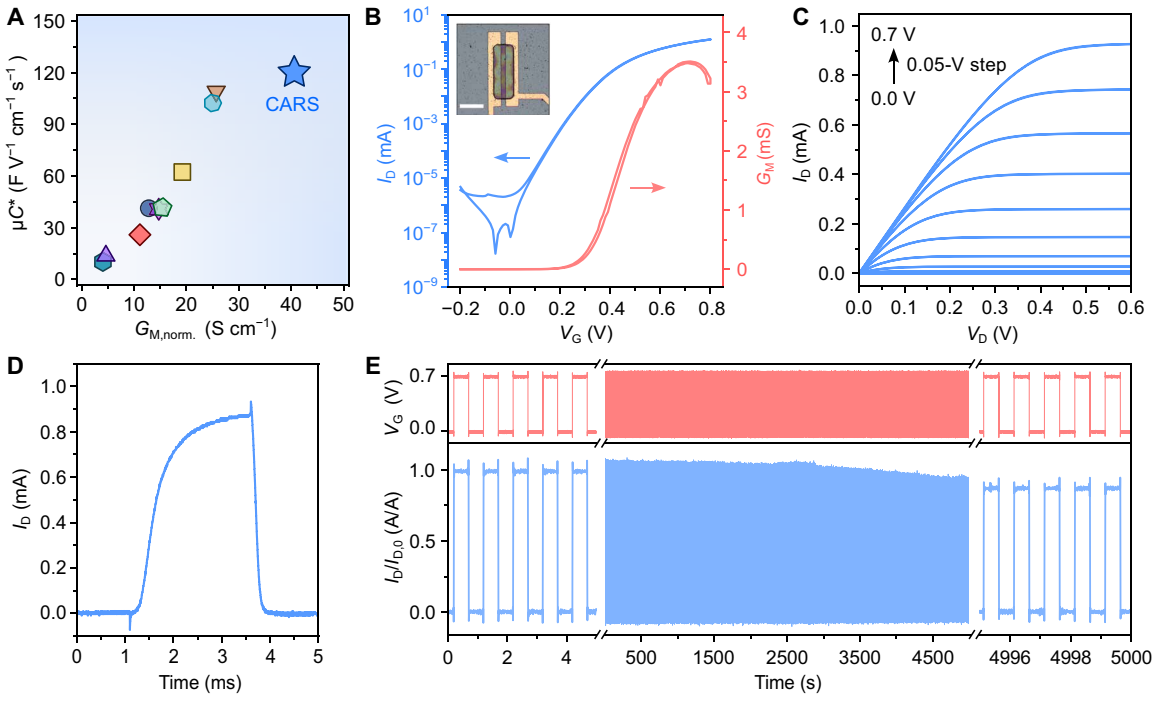

Fig. 3. Electrical characterization of OECT devices. (**A**) Comparison of transconductance and mobility × volumetric capacitance (μC*) of CARS and previously reported n-type organic semiconducting polymers (*25*–*31*). See Table S3 for detailed information on the properties of the compared systems. (**B**) Typical transfer characteristics and transconductance of CARS-based OECT. Device dimensions: 100 μm/10 μm. V_D = 0.6 V. Photo inset depicts top-view microscopy photograph of the channel region of a CARS-based OECT. Scale bar, 50 μm. (**C**) Typical output characteristics of CARS-based OECT. (**D**) Temporal response of the drain current of a CARS-based OECT in response to a 0.7 V square wave V_G pulse. V_D = 0.65 V. Time constants were obtained from fitting the current response to an exponential function. (**E**) Switching stability of CARS OECT under ambient conditions. A square-wave V_G pulse of 0.7 V was applied at 1 Hz for more than 5000 cycles.

defects in D-CARS introduce rotatable bonds between neighboring units that limit π-π overlap and disrupt efficient conjugation through the backbone (Fig. 1B), consistent with our observations regarding solution-phase absorption spectra (Fig. 4C). In addition, while both CARS and D-CARS have similar morphologies and packing in the solid state (figs. S12 and S13), these defects can disrupt π-π stacking between neighboring ribbons and introduce electron trap states that limit intermolecular electron hopping (*36*, *37*). Together, our results show that the design principle for high-performance OMIECs is to build in structural integrity to optimize efficient charge transport.

The CARS platform is highly versatile as biosensors. We demonstrate here their utility in implantable neural probes in a rodent brain. The devices are sensitive to cations and the implanted devices are nontoxic, biocompatible, and stable over weeks at a time. The basis for this sensor is a defect-free ribbon structure that promotes both high ion and high electron transport. Given the easily functionalizable nature of the CARS platform, they will be broadly deployable as in vivo biosensors. In addition, as an n-type material on par with leading p-type OMIECs, CARS can play a key role in the development of complementary circuitry for applications such as electrophysiological amplifiers, neuromorphic computing, and artificial spiking networks (*23*).

MATERIALS AND METHODS

Materials

All reagents and anhydrous solvents were obtained from Sigma-Aldrich and used as received unless otherwise specified. Synthetic scheme of CARS is depicted in Fig. 1D. See the Supplementary Materials for detailed synthetic procedures. PEDOT:PSS (Clevios PH1000) was purchased from Heraeus and enhanced by 20% (v/v) ethylene glycol, 0.6% (v/v) acetic acid, and crosslinked with the addition of 1% (v/v) (3-glycidyloxypropyl)trimethoxysilane.

Conformable probe fabrication

Silicon wafers (100 mm in diameter; single side polish, 550 μm in thickness) were coated with an anti-adhesion layer consisting of 0.3% soap through a spin coating process at 1500 rpm for 30 s. A 2-μm parylene-C layer was deposited through chemical vapor deposition using a Specialty Coating Systems Labcoter 2. A metal layer consisting of 10-nm titanium and 150-nm gold was patterned through optical lithography using nLOF 2020 negative photo resist spun at 3000 rpm for 30 s and pre- and post-exposure baked at 110°C for 90 s before developing in AZ 300MIF for 120 s. An Angstrom EvoVac multiprocess evaporator was used to deposit metals via electron beam evaporation, and the patterned resist and excess metal was removed in an acetone liftoff process. A second 2-μm parylene-C layer was deposited with the inclusion of A-174 silane as an adhesion promotor. An additional 2-μm parylene-C layer was deposited without adhesion promotor after the spin coating of an antiadhesion layer of 5% soap at 1500 rpm for 30 s. AZ 10XT–positive photoresist was applied and patterned by spin coating at 300 rpm for 10 s and 5000 rpm for 30 s and then pre-exposure baking at 110°C for 90 s. The resist was developed in two 20% (v/v) diluted baths of AZ 400K in deionized water for 210 s each. Parylene-C layers were then etched with an oxygen plasma reactive ion etching process [180 W, 50 s.c.c.m.

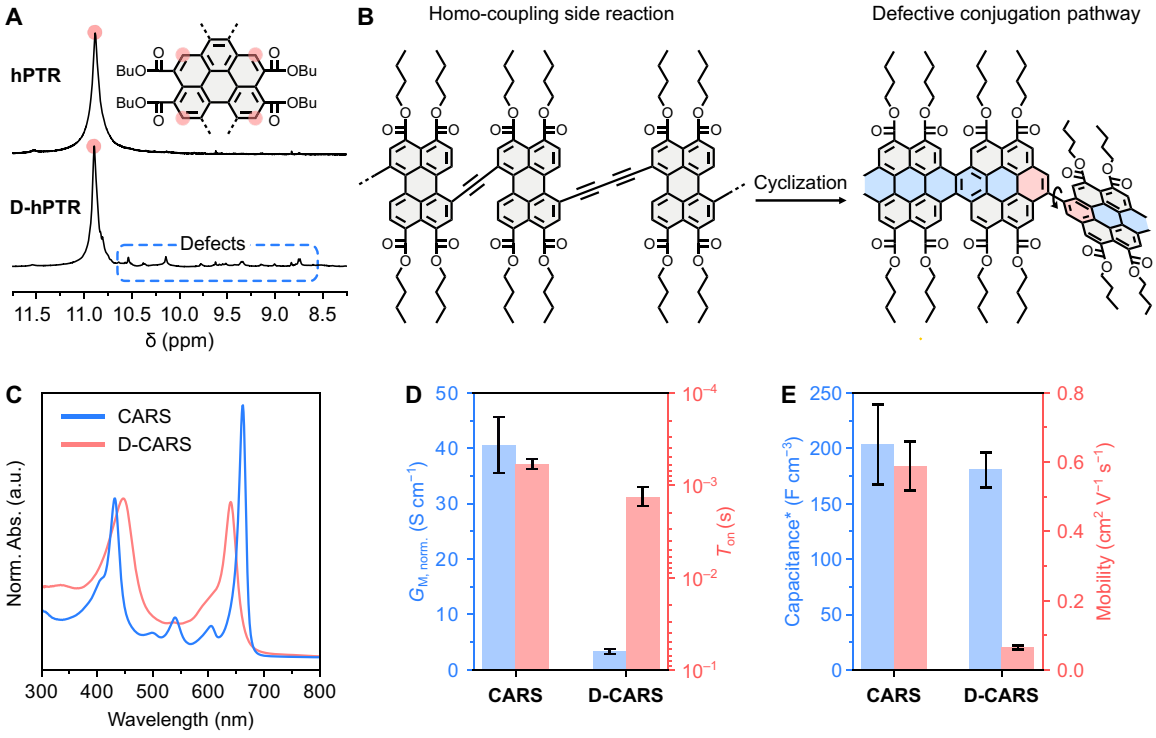

Fig. 4. Comparison of defect-free and defect-containing CARS. (**A**) Comparison of the aromatic region of the ^{1}H NMR spectra of hPTR (top) and D-hPTR (bottom). Resonances assigned to the ortho-protons on the perylene units are highlighted. (**B**) Disruptive conjugation in the acene ribbon backbone arising from homo-coupling side reactions during the Stille cross-coupling. (**C**) Normalized UV-vis absorption spectra of CARS (blue) and D-CARS (pink) in hexafluoroisopropanol. (**D**) Comparison of transconductance and temporal response of CARS and D-CARS. Mean values are reported ± SD. $N = 10$ transistors (**E**) Comparison of volumetric capacitance and electron mobility of CARS and D-CARS. Capacitance* calculated from linear fit in fig. S8E ± SD. $N = 3$ electrodes. Mobility values are mean ± SD. $N = 10$ transistors.

(standard cubic centimeters per minute) of O_2 and 2 s.c.c.m. of SF_6; Oxford Plasmalab 80] for 13.5 min. The CARS polymer solution was spin-coated at 5000 rpm for 30 s before being baked for 2 min at 110°C. The top layer of parylene-C was then peeled off to pattern the polymer, and the probes were removed from the silicon wafer with the assistance of deionized water.

OECT fabrication and characterization

Metal contacts and interconnects (10 nm Ti/150 nm Au) were patterned onto silica substrates using a metal lift-off process. Then, a 2-μm layer of parylene-C was deposited with a 3-(trimethoxysilyl) propyl methacrylate (A-174 Silane) adhesion promoter using an SCS Labcoter 2. An anti-adhesion agent, 5 weight % Micro-90 diluted in deionized water, was spin-coated onto the wafers at 1500 rpm before deposition of another 2-μm parylene-C. The parylene-C was patterned using AZ 10XT photoresist and etched by reactive ion etching with O_2 plasma (180 W, 50 s.c.c.m. of O_2 and 2 s.c.c.m. of SF_6; Oxford Plasmalab 80). The CARS polymer solution (15 mg/ml in hexafluoroisopropanol) was spin-coated onto the devices at 5000 rpm for 60 s before peeling off the second parylene-C layer. The devices were measured with 1× phosphate-buffered saline as an electrolyte and Ag/AgCl as gate electrodes. Transfer and output characteristics were characterized using a Keithley 4200 SCS analyzer. Temporal measurements were taken using a RIGOL DHO924S Oscilloscope. A Keysight 33500B series function generator and a Keysight B2902A Precision Source Measurement Unit were used to provide the input and drain voltage, respectively.

Animal surgical procedure

Animal experiments were approved by the Institutional Animal Care and Use Committee of Columbia University. Adult male Long Evans rats were anesthetized with 2% isoflurane and maintained under anesthesia with 1% isoflurane for intracranial implantation of the conducting polymer-based NeuroGrid. The electrocorticography array was placed on the cortical surface of the brain, and screws in the skull were used as ground electrodes. Rats recovered for 4 days before the first recording.

Neurophysiological data and processing

Neural data were acquired through a custom-printed circuit board incorporating an Intan RHD2000 system and bonded to the conformable probe using mixed conducting particulate 3. Data were recorded continuously at 20 kHz and later analyzed using MATLAB (MathWorks) and NeuroScope. Impedance measurements were performed using the Intan impedance self-test function at 1 kHz and a Gamry 600+ Potentiostat in the three-electrode configuration.

Supplementary Materials

This PDF file includes:

Experimental Details
Figs. S1 to S27
Tables S1 to S3
Computational Results
References

REFERENCES AND NOTES

1. J. Rivnay, S. Inal, A. Salleo, R. M. Owens, M. Berggren, G. G. Malliaras, Organic electrochemical transistors. *Nat. Rev. Mater.* **3**, 17086 (2018).
2. J. Rivnay, H. Wang, L. Fenno, K. Deisseroth, G. G. Malliaras, Next-generation probes, particles, and proteins for neural interfacing. *Sci. Adv.* **3**, e1601649 (2017).
3. Y. Wang, S. Wustoni, J. Surgailis, Y. Zhong, A. Koklu, S. Inal, Designing organic mixed conductors for electrochemical transistor applications. *Nat. Rev. Mater.* **9**, 249–265 (2024).
4. S. Inal, J. Rivnay, A.-O. Suiu, G. G. Malliaras, I. McCulloch, Conjugated Polymers in Bioelectronics. *Acc. Chem. Res.* **51**, 1368–1376 (2018).
5. Z. D. Kojabad, S. A. Shojaosadati, S. M. Firoozabadi, S. Hamedi, Polypyrrole nanotube modified by gold nanoparticles for improving the neural microelectrodes. *J. Sol. State Electrochem.* **23**, 1533–1539 (2019).
6. X. Liu, Z. Yue, M. J. Higgins, G. G. Wallace, Conducting polymers with immobilised fibrillar collagen for enhanced neural interfacing. *Biomaterials* **32**, 7309–7317 (2011).
7. Y. Jiang, Z. Zhang, Y.-W. Wang, D. Li, C.-T. Coen, E. Hwuan, G. Chen, H.-C. Wu, D. Zhong, S. Niu, W. Wang, A. Saberi, J.-C. Lai, Y. Wu, Y. Wang, A. A. Trotsyuk, K. Y. Loh, C.-C. Shih, W. Xu, L. K. Zhang, Y. Bai, G. Gurusankar, W. Hu, W. Jia, Z. Cheng, R. H. Dauskardt, G. C. Gurtner, J. B.-H. Tok, K. Deisseroth, I. S. Soltesz, Z. Bao, Topological supramolecular network enabled high-conductivity, stretchable organic bioelectronics. *Science* **375**, 1411–1417 (2022).
8. D. Khodagholy, T. Doublet, M. Gurfinkel, P. Quilichini, E. Ismailova, P. Leleux, T. Herve, S. Sanaur, C. Bernard, G. G. Malliara, Highly conformable conducting polymer electrodes for in vivo recordings. *Adv. Mater.* **23**, H268–H273 (2011).
9. C.-Y. Lo, Y. Wu, E. Awuyah, D. Meli, D. M. Nguyen, R. Wu, B. Xu, J. Strzalka, J. Rivnay, D. C. Martin, L. V. Kayser, Influence of the molecular weight and size distribution of PSS on mixed ionic-electronic transport in PEDOT:PSS. *Polym. Chem.* **13**, 2764–2775 (2022).
10. G. D. Spyropoulos, J. N. Gelinas, D. Khodagholy, Internal ion-gated organic electrochemical transistor: A building block for integrated bioelectronics. *Sci. Adv.* **5**, eaau7378 (2019).
11. Z. Chen, X. Ding, L. Wang, X. Guo, S. Shao, K. Feng, π-Conjugated polymers for high-performance organic electrochemical transistors: Molecular design strategies, applications and perspectives. *Angew. Chem. Int. Ed.* **64**, e202423013 (2025).
12. Y. Zhong, B. Kumar, S. Oh, M. T. Trinh, Y. Wu, K. Elbert, P. Li, X. Zhu, S. Xiao, F. Ng, M. L. Steigerwald, C. Nuckolls, Helical ribbons for molecular electronics. *J. Am. Chem. Soc.* **136**, 8122–8130 (2014).
13. Z. Jin, C. Qian, S. T. Bao, R. Zhang, A. M. Evans, F. Ng, Y. Xu, M. L. Steigerwald, A. E. McDermott, Y. Yang, C. Nuckolls, Iterative synthesis of contorted macromolecular ladders for fast-charging and long-life lithium batteries. *J. Am. Chem. Soc.* **144**, 13973–13980 (2022).
14. C. Schaack, A. M. Evans, F. Ng, M. L. Steigerwald, C. Nuckolls, High-performance organic electronic materials by contorting perylene diimides. *J. Am. Chem. Soc.* **144**, 42–51 (2022).
15. S. T. Bao, H. Jiang, C. Schaack, S. Louie, M. L. Steigerwald, C. Nuckolls, Z. Jin, Remote control of dynamic twistacene chirality. *J. Am. Chem. Soc.* **144**, 18772–18777 (2022).
16. J. C. Russell, V. A. Posey, J. Gray, R. May, D. A. Reed, H. Zhang, L. E. Marbella, M. L. Steigerwald, Y. Yang, X. Roy, C. Nuckolls, S. R. Peurifoy, High-performance organic pseudocapacitors via molecular contortion. *Nat. Mater.* **20**, 1136–1141 (2021).
17. T. Nguyen-Dang, S. T. Bao, C. Kaiyasuan, K. Li, S. Chae, A. Yi, S. Joy, K. Harrison, J. Y. Kim, F. Pallini, L. Beverina, K. R. Graham, C. Nuckolls, T. Q. Nguyen, Air-stable perylene diimide trimer material for N-type organic electrochemical transistors. *Adv. Mater.* **36**, 2312254 (2024).
18. Y. Yu, G. Zhu, L. Lan, L. Chen, X. Zhu, J. Duan, S. Cong, Z. Li, Y. Wang, Z. Wang, I. McCulloch, W. Yue, n-type glycolated imide-fused polycyclic aromatic hydrocarbons with high capacity for liquid/solid-electrolyte-based electrochemical devices. *Adv. Funct. Mater.* **33**, 2300012 (2023).
19. A. R. Hassan, Z. Zhao, J. J. Ferrero, C. Cea, P. Jastrzebska-Perfect, J. Myers, P. Asman, N. F. Ince, G. McKhann, A. Viswanathan, S. A. Sheth, D. Khodagholy, J. N. Gelinas, Translational organic neural interface devices at single neuron resolution. *Adv. Sci.* **9**, 2202306 (2022).
20. D. Khodagholy, J. Rivnay, M. Sessolo, M. Gurfinkel, P. Leleux, L. H. Jimison, E. Stavrinidou, T. Herve, S. Sanaur, R. M. Owens, G. G. Malliaras, High transconductance organic electrochemical transistors. *Nat. Commun.* **4**, 2133 (2013).
21. G. Buzsáki, *Rhythms of the Brain* (Oxford Univ. Press, 2011).
22. T. Harmony, The functional significance of delta oscillations in cognitive processing. *Front. Integr. Neurosci.* **7**, 83 (2013).
23. D. J. Wisniewski, L. Ma, O. J. Rauhala, C. Cea, Z. Zhao, A. Ranschaert, J. N. Gelinas, D. Khodagholy, Spatial control of doping in conducting polymers enables complementary, conformable, implantable internal ion-gated organic electrochemical transistors. *Nat. Commun.* **16**, 517 (2025).
24. I. Uguz, D. Ohayon, S. Yilmaz, S. Griggs, R. Sheelamanthula, J. D. Fabbri, I. McCullouch, S. Inal, K. L. Shepard, Complementary integration of organic electrochemical transistors for front-end amplifier circuits of flexible neural implants. *Sci. Adv.* **10**, eadi9710 (2024).
25. H.-Y. Wu, C.-Y. Yang, Q. Li, N. B. Kolhe, X. Strakosas, M.-A. Stoeckel, Z. Wu, W. Jin, M. Savvakis, R. Kroon, D. Tu, H. Y. Woo, M. Berggren, S. A. Jenekhe, S. Fabiano, Influence of molecular weight on the organic electrochemical transistor performance of ladder-type conjugated polymers. *Adv. Mater.* **34**, 2106235 (2022).
26. Y. Wang, A. Koklu, Y. Zhong, T. Chang, K. Guo, C. Zhao, T. C. Hidalgo Castillo, Z. Bu, C. Xiao, W. Yue, W. Ma, S. Inal, Acceptor functionalization via green chemistry enables high-performance n-type organic electrochemical transistors for biosensing, memory applications. *Adv. Funct. Mater.* **34**, 2304103 (2024).
27. Z. Huang, P. Li, Y. Lei, X.-Y. Deng, Y.-N. Chen, S. Tian, X. Pan, X. Lei, C. Song, Y. Zheng, J.-Y. Wang, Z. Zhang, T. Lei, Azonia-Naphthalene: A cationic hydrophilic building block for stable n-type organic mixed ionic-electronic conductors. *Angew. Chem. Int. Ed.* **63**, e202313260 (2024).
28. K. Feng, W. Shan, J. Wang, J.-W. Lee, W. Yang, Wu, Y. Wang, B. J. Kim, X. Guo, H. Guo, Cyano-functionalized n-type polymer with high electron mobility for high-performance organic electrochemical transistors. *Adv. Mater.* **34**, 2201340 (2022).
29. P. Li, J. Shi, Y. Lei, Z. Huang, T. Lei, Switching p-type to high-performance n-type organic electrochemical transistors via doped state engineering. *Nat. Commun.* **13**, 5970 (2022).
30. K. Feng, W. Shan, S. Ma, Z. Wu, J. Chen, H. Guo, B. Liu, J. Wang, B. Li, H. Y. Woo, S. Fabiano, Fused bithiophene imide dimer-based n-type polymers for high-performance organic electrochemical transistors. *Angew. Chem. Int. Ed.* **60**, 24198–24205 (2021).
31. S. Cong, J. Chen, M. Xie, Z. Deng, C. Chen, R. Liu, J. Duan, X. Zhu, Z. Li, Y. Cheng, W. Huang, I. McCullouch, W. Yue, Single ambipolar OECT–based inverter with volatility and nonvolatility on demand. *Sci. Adv.* **10**, eadq9405 (2024).
32. P. Li, W. Sun, J. Li, J.-P. Chen, X. Wang, Z. Mei, G. Jin, Y. Lei, R. Xin, M. Yang, J. Xu, X. Pan, C. Song, X.-Y. Deng, X. Lei, K. Liu, X. Wang, Y. Zheng, J. Zhu, S. Lv, Z. Zhang, X. Dai, T. Lei, N-type semiconducting hydrogel. *Science* **384**, 557–563 (2024).
33. G. Buzsáki, A. Draguhn, Neuronal oscillations in cortical networks. *Science* **304**, 1926–1929 (2004).
34. J. S.-J. Yang, L. Fang, Conjugated ladder polymers: Advances from syntheses to applications. *Chem* **10**, 1668–1724 (2024).
35. S. T. Bao, S. Louie, H. Jiang, Q. Jiang, S. Sun, M. L. Steigerwald, C. Nuckolls, Z. Jin, Near-infrared, organic chiroptic switch with high dissymmetry factors. *J. Am. Chem. Soc.* **146**, 51–56 (2024).
36. B. Ma, Q. Shi, X. Ma, Y. Li, H. Chen, K. Wen, R. Zhao, F. Zhang, Y. Lin, Z. Wang, H. Huang, Defect-free alternating conjugated polymers enabled by room-temperature stille polymerization. *Angew. Chem. Int. Ed.* **61**, e202115969 (2022).
37. H. Xiong, Q. Lin, Y. Lu, D. Zheng, Y. Li, S. Wang, W. Xie, C. Li, X. Zhang, Y. Lin, Z.-X. Wang, Q. Shi, T. J. Marks, H. Huang, General room-temperature Suzuki–Miyaura polymerization for organic electronics. *Nat. Mater.* **23**, 695–702 (2024).
38. M. Shahi, V. N. Le, P. A. Espejo, M. Alsufyani, C. J. Kousseff, I. McCulloch, A. F. Paterson, The organic electrochemical transistor conundrum when reporting a mixed ionic–electronic transport figure of merit. *Nat. Mater.* **23**, 2–8 (2024).
39. D. A. Bernards, G. G. Malliaras, Steady-state and transient behavior of organic electrochemical transistors. *Adv. Funct. Mater.* **17**, 3538–3544 (2007).
40. Z. Yuan, Y. Xiao, Z. Li, X. Qian, Efficient synthesis of regioisomerically pure bis(trifluoromethyl) substituted 3,4,9,10-perylene tetracarboxylic bis(benzimidazole). *Org. Lett.* **11**, 2808–2811 (2009).
41. K. Gu, J. Onorato, S. S. Xiao, C. K. Luscombe, Y.-L. Loo, Determination of the molecular weight of conjugated polymers with diffusion ordered NMR spectroscopy. *Chem. Mater.* **30**, 570–576 (2018).
42. W. Li, H. Chung, C. Daeffler, J. A. Johnson, R. H. Grubbs, Application of ^{1}H DOSY for facile measurement of polymer molecular weights. *Macromolecules* **45**, 9595–9603 (2012).
43. A. D. Bochevarov, E. Harder, T. F. Hughes, J. R. Greenwood, D. A. Braden, D. M. Philipp, D. Rinaldo, M. D. Halls, J. Zhang, R. A. Friesner, Jaguar: A high-performance quantum chemistry software program with strengths in life and materials sciences. *Int. J. Quant. Chem.* **113**, 2110–2142 (2013).

Acknowledgments: We acknowledge the use of facilities and instrumentation supported by NSF through the Columbia University, Columbia Nano Initiative, and the Materials Research Science and Engineering Center DMR-2011738. We would like to thank J. Vichiconti, Y. Borisenkov, D. Cardinal, P. Chow, and N. Ariel-Sternberg (CNI), as well as K. Lee, D. Cavlovic, and H. Jiang for valuable discussions. **Funding:** C.N. thanks S. Buckler and D. Buckler for the generous support. The NMR measurements reported in this publication was supported by the Office of The Director of the National Institutes of Health under award number S10OD026749. The content is solely the responsibility of the authors and does not necessarily represent the official views of the National Institutes of Health. This research used the Complex Materials Scattering (CMS) 11-BM beamline of the National Synchrotron Light Source II, a US Department of Energy (DOE) Office of Science User Facility operated for the DOE Office of Science by Brookhaven National Laboratory under contract no. DE-SC0012704. **Author contributions:** S.L., Q.J., M.S., and C.N. designed the material. Q.J., S.T.B., and F.N. developed

the synthesis method. S.R.D. assisted with NMR characterization. S.L. and D.J.W. fabricated and characterized the devices. D.J.W. and D.K. performed the electrophysiology in vivo experiments and analysis. H.Z., K.C, Q.F., A.G., and Y.Z. assisted with thin-film characterization. All authors contributed to writing the paper. **Competing interests:** S.L., Q.J., D.J.W., Y.Z., F.N., D.K., and C.N. have filed a US Patent and Trademark Office provisional patent application related to this work (application serial number: 63/725,812; filed 27 November 2024). The other authors declare that they have no competing interests. **Data and materials availability:** All data needed to evaluate the conclusions in the paper are present in the paper and/or the Supplementary Materials.

Submitted 29 October 2024
Accepted 27 February 2025
Published 2 April 2025
10.1126/sciadv.adu2356